Nitrogen Fixation by Ru Single-Atom Electrocatalytic Reduction

Hengcong Tao,[a] Zishan Han,[a] Changhyeok Choi,[b] Mingwen Jia,[a] Qun Fan,[a] Yunnan Gao,[a] Alex W. Robertson,[c] Song Hong,[a] Yousung Jung,*[b] Shizhen Liu[a] and Zhenyu Sun*[a]

[a] State Key Laboratory of Organic-Inorganic Composites, Beijing University of Chemical Technology, Beijing 100029, China. E-mail: sunzy@mail.buct.edu.cn
[b] Graduate School of EEWS, Korea Advanced Institute of Science and Technology (KAIST) Daejeon 34141, Republic of Korea. E-mail: ysjn@kaist.ac.kr
[c] Department of Materials, University of Oxford, Oxford OX1 3PH, United Kingdom

SUMMARY

Nitrogen fixation under ambient conditions remains a significant challenge. In this work, we report nitrogen fixation by Ru single-atom electrocatalytic reduction at room temperature and atmospheric pressure. In contrast to traditional Ru nanoparticles, we show that single Ru sites supported on ZrO_2/N-doped porous carbon greatly promoted electroreduction of aqueous N_2 selectively to NH_3, affording an NH_3 faradaic efficiency of about 21% at a very low overpotential (0.206 V), which significantly surpasses other reported catalysts. An unprecedented NH_3 formation rate of 4560 $\mu g \cdot h^{-1}$ $mg^{-1}{}_{Ru}$ was achieved at -0.21 V versus a reversible hydrogen electrode at room temperature and pressure, with stable behavior for at least 60 h of reaction. Comparable results would ordinarily require high temperatures and/or pressures. . Experiments combined with density functional calculations showed that the Ru sites with oxygen vacancies were major active centres that permited the stabilization of *NNH, the dramatic destabilization of *H, and enhanced N_2 adsorption.

INTRODUCTION

The reduction of N_2 to NH_3 at room temperature and atmospheric pressure has been the subject of intense research. However, the N_2 molecule is stable and inert, with a strong triple-bond and low polarizability.[1,2] The Haber-Bosch process that was developed 100 years ago is still employed in industry for NH_3 synthesis at high temperatures (> 300 °C) and pressures (> 10 MPa).[3] This energy- and capital-intensive process uses H_2 that is mainly produced from the steam reformation of natural gas, which substantially increases greenhouse gas emissions.[3] Additionally, the NH_3 yield is rather low with a conversion of less than 15%. Finding efficient ways to adsorb and activate N_2 remains a big challenge.

Electrochemical reduction of N_2 to NH_3 is an attractive route, and can be powered by energy from solar or wind sources, enabling a sustainable energy economy.[4] There are two major issues associated with electrochemical N_2 reduction: (1) large overpotential and (2) low faradaic efficiency (FE) toward NH_3 due to occurrence of the competing hydrogen evolution reaction (HER), especially in aqueous solutions.[5,6] So far, only a limited number of electrocatalysts (Au,[7-9] Pt/C,[10] Ru,[11] Mo,[6] Ag/Au,[12] $Bi_4V_2O_{11}/CeO_2$,[13] Rh,[14] and Fe/CNT[15]) have been reported for reduction of N_2 to NH_3. Most of these catalysts, however, suffer from slow reaction kinetics, low N_2 adsorption and reduction activity. The highest NH_3 FE reported hitherto in ambient aqueous N_2 electroreduction reaction (NRR) is about 10.1% at -0.48 V versus (*vs.*) Ag/AgCl for amorphous Au supported on CeO_x/reduced graphene oxide.[7] Ru is considered as a second-generation NH_3 catalyst with a N_2 reduction potential calculated to be lower than Fe.[4,11,16] However, to-date only one work has demonstrated NH_3 production on Ru cathodes, with a NH_3 formation rate and FE in the best case being limited to 1.3 $\mu g\ h^{-1}\ cm^{-2}$ (at -1.02 V *vs.* Ag/AgCl) and 0.92% (at -0.96 V *vs.* Ag/AgCl) at 90 °C, respectively.[11] Despite these advances, high FE is usually obtained at the expense of low NH_3 production rate. Therefore, designing selective and energy-efficient electrocatalysts is highly desirable to enable both high FE and NH_3 synthesis rate at low overpotentials.

Isolated metal atoms that are dispersed on supports[17] have attracted tremendous interest owing to the homogeneity of the catalytically active sites, low-coordination environment of metal atoms, and maximum metal utilization efficiency. These important features endow single atom catalysts with high catalytic activity, stability, and selectivity for a range of electrochemical processes.[18] Nevertheless, single-atom electrocalysis in NH_3 synthesis has yet to be reported. Here, we show for the first time that single Ru sites encapsulated in ZrO_2/N doped porous carbon (Ru@ZrO_2/NC) via a coordination-assisted strategy enable highly efficient electrochemical N_2 fixation. Control of coordinated ligands permits ready tuning of Ru sizes and catalytic properties of Ru in NRR. Importantly, this catalyst provided an unprecedentedly high NH_3 yield rate of 4560 $\mu g \cdot h^{-1}\ mg^{-1}_{Ru}$ at -0.21 V *vs.* reversible hydrogen electrode (RHE), which is over 3 times higher than that of the best reported catalyst, Au/TiO_2.[9] A very high NH_3 FE of approximately 21% was also achieved even at a low applied potential of -0.11 V, outperforming other metal-based catalysts, and comparable to the yields and efficiencies attained under harsh temperatures and/or pressures.

RESULTS AND DISCUSSION

UiO-66 [$Zr_6O_4(OH)_4(BDC)_6$, BDC: 1,4-benzenedicarboxylate] confined with Ru ions was first synthesized simply by a hydrothermal method, which was subsequently annealed to yield Ru@ZrO_2/NC. Inductively Coupled Plasma-Atomic Emission Spectrometry (ICP-AES) verified the existence of Ru in the resultant samples. The X-ray diffraction (XRD) patterns of these samples are given in Figure S1 (Supporting Information). Characteristic reflection peaks of ZrO_2 were observed in the resulting Ru@ZrO_2/NC. The average ZrO_2 sizes were estimated to be about 9 nm from the (111) reflection utilizing Scherrer's equation. No diffraction peaks of Ru were identified, probably due to its amorphous structure and/or too low loading content (0.1 wt% determined by ICP-AES). This also ruled out the presence of large Ru particles or aggregates.

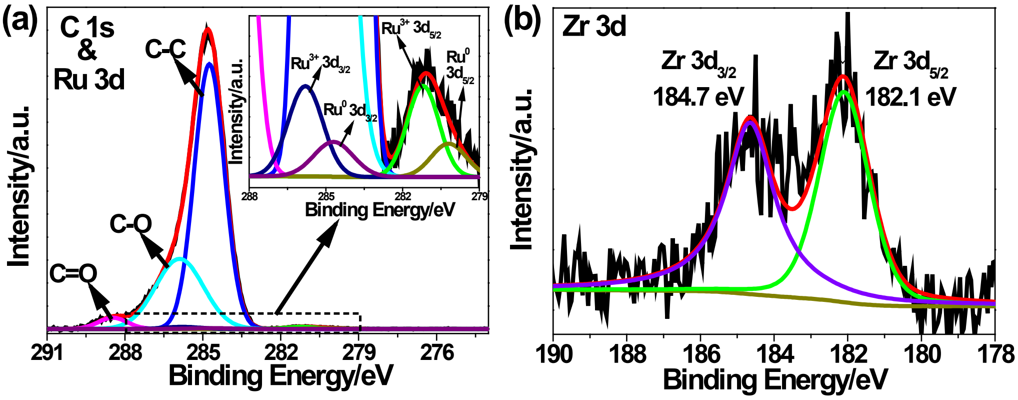

Figure 1. Surface Characterization by XPS

(a) C 1s and Ru 3d XPS spectra of Ru@NC.

(b) Zr 3d XPS spectrum of Ru@ZrO_2/NC.

The formation of Ru was also confirmed by the presence of Ru 3d X-ray photoelectron spectroscopy (XPS) signal which is obscured by the C 1s signal at 284.8 eV (Figure 1a). The deconvoluted spectrum presents two doublets, denoting a main valence state of Ru^{3+} together with Ru^0. The peaks at 284.8, 285.9, and 288.5 eV correspond to C–C bonds in aromatic networks, C–O bonds in phenols or ethers, and C=O groups in ketones and quinones, respectively. The Zr 3d core level spectrum (Figure 1b) shows a Zr $3d_{5/2}$ peak at 182.1 eV which is lower than the value of ZrO_2 (182.8 eV) reported in literature.[14] This may suggest the generation of oxygen vacancies on the surface of ZrO_2 as a result of annealing in N_2. Pyridinic N and pyrrolic N were observed to be predominant N species in the Ru@ZrO_2/NC (Figure S2). These two N moieties facilitated the yield and stabilization of Ru atoms by coordination with the metal.[19] N doping also introduced defect sites in the carbon lattice, thus affecting catalytic properties which will be discussed later on in the NRR part.

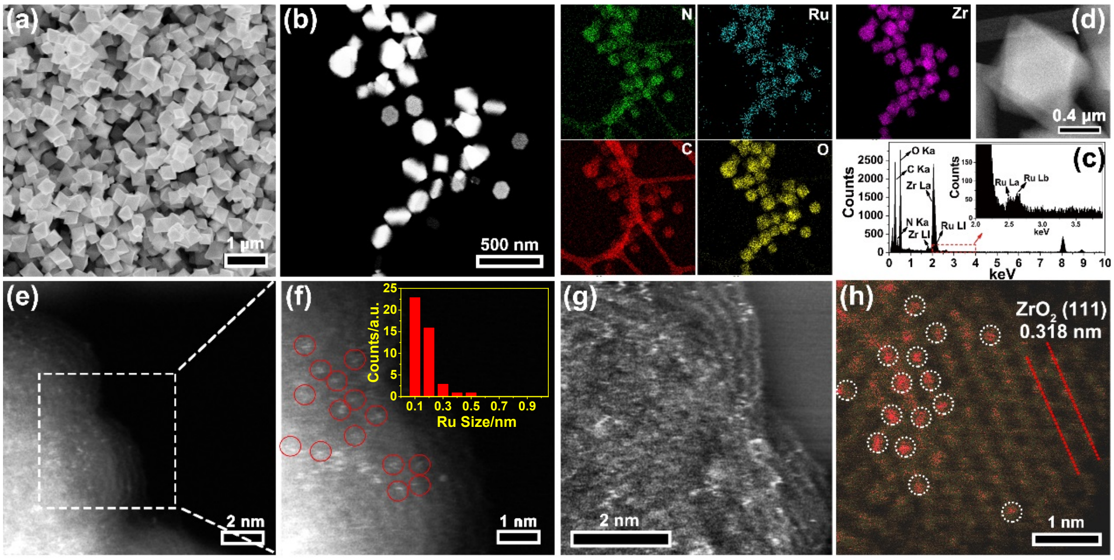

Figure 2. Morphology and Structure Characterization of Ru@ZrO_2/NC

(a) SEM image.

(b) Low-magnification HAADF-STEM image along with EDS maps of C, N, Ru, Zr, and O.

(c) EDX spectrum of the region shown in image b.

(d)-(h) HAADF-STEM images. The Inset in image f showed the size-distribution histogram of Ru objects. Image g has been subjected to a bandpass filter to remove the variations in intensity due to the differing carbon support thicknesses, allowing for clearer distinguishing of the Ru single atoms.

Scanning electron microscopy (SEM) (Figure 2a and Figure S3) and aberration corrected high-angle annular dark-field scanning transmission electron microscopy (HAADF-STEM) images (Figures 2b and d) showed octahedron morphology of the Ru@ZrO_2/NC, similar to the shape of UiO-66-NH_2. In-situ energy-dispersive X-ray spectroscopy (EDS) together with elemental mapping (Figure 2c) and HAADF-STEM observation confirmed the distribtution of single Ru sites on the carbon support. Brighter spots in the HAADF-STEM images indicate single Ru atoms, due to the atomic number contrast nature of the technique and the higher atomic number of Ru compared to C (Figures 2e-g). For clarity, some Ru atoms are annotated with red circles (Figure 2f). The sizes of about 88% of Ru objects fell in the range of 0.1-0.2 nm (inset of Figure 2f), corresponding to single atoms. The formation of such atomically dispersed Ru is most likely due to the stabilization of $RuCl_3$ precursor by the uncoordinated –NH_2 groups and further inhibition of Ru assembling during pyrolysis. By contrast, Ru clusters were obtained originating from aggregation of Ru atoms at high temperature in the absence of −NH_2 groups (Figure S4). This suggests the importance of −NH_2 groups in the yield of Ru single sites during the annealing process. Additionally, some Ru atoms dispersed on ZrO_2 were also visualized by virtue of the higher atomic number of Ru than Zr and O (Figure 2h).

The N_2 reduction activities of all catalysts were tested in a typical three-electrode electrochemical system. Figure 3a shows the linear sweep voltammetries (LSVs) of Ru@ZrO_2/NC in 0.1 M aqueous HCl solution saturated with Ar or N_2, respectively. The NRR takes place at potentials > -0.01 V under N_2 saturation at room temperature and atmospheric pressure when using Ru@ZrO_2/NC as the cathodic catalyst. Such an onset potential is similar to that of Au subnanoclusters on TiO_2, but significantly more positive than the value attained on N-doped porous carbon catalyst (-0.38 V *vs.* RHE).[20] Under reaction conditions, only NH_3 was detected by the indophenol blue method. No by-product N_2H_4 was detectable by the Watt and Chrisp method, suggesting good selectivity of Ru@ZrO_2/NC for NRR.

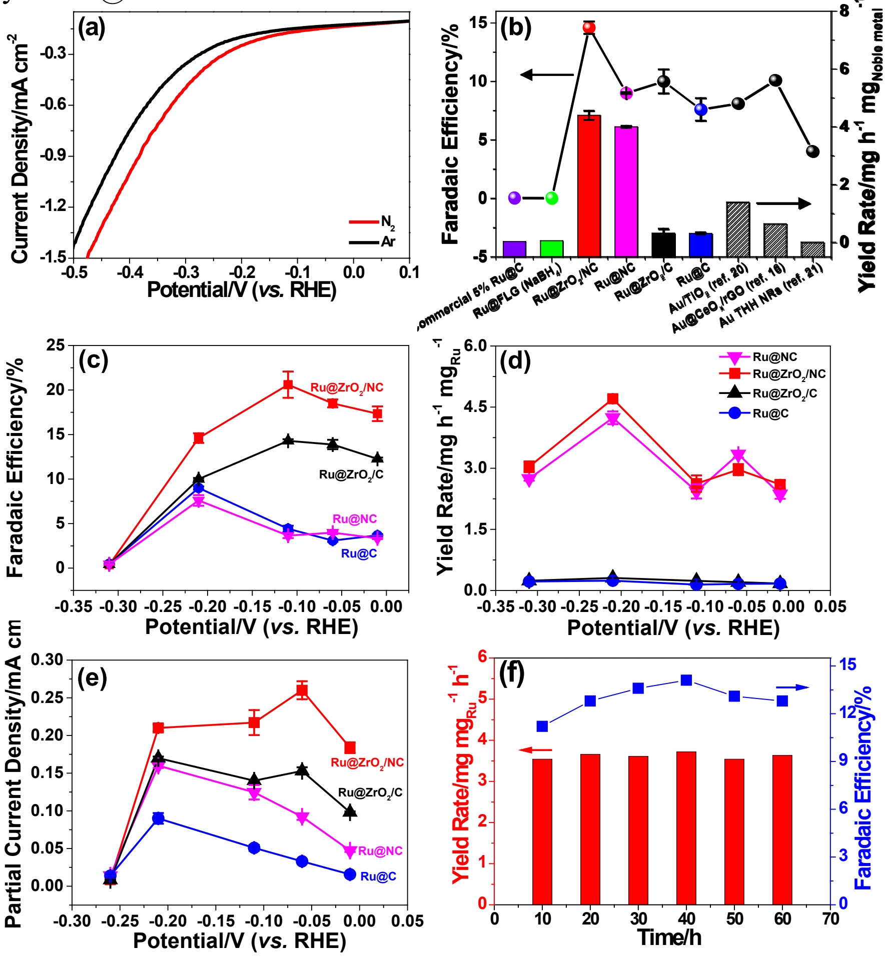

Figure 3. Electrochemical Nitrogen Reduction Activities

(a) The LSVs of Ru@ZrO_2/NC in Ar- or N_2-saturated 0.1 M HCl at a scan rate of 5 mV s^{-1}.

(b) The FE and yield rate of NH_3 over 5% Ru@C, Ru@FLG ($NaBH_4$), Ru@ZrO_2/NC, Ru@NC (removal of ZrO_2), Ru@ZrO_2/C (in the absence of $-NH_2$ groups), and Ru@C (in the absence of $-NH_2$ groups & removal of ZrO_2). The results of Au catalysts[7-9] reported earlier were also provided for comparison. The NH_3 yield rates were normalized by dividing corresponding noble metal mass.

(c) The FEs, (d) yield rates, and (e) partial current densities of NH_3 over Ru@NC, Ru@C, Ru@ZrO_2/NC, and Ru@ZrO_2/C at various applied potentials.

(f) The long-term durability test at -0.21 V (*vs.* RHE) over Ru@ZrO_2/NC at ~10 °C.

Interestingly, as shown in Figure 3b, the Ru@ZrO_2/NC catalyst displayed an NH_3 yield rate of up to 4560 $\mu g \cdot h^{-1}$ mg^{-1}_{metal} at -0.21 V, over 3 times higher than that of the best catalyst (Au/TiO_2) reported so far.[9] The NH_3 FE of Ru@ZrO_2/NC at -0.21 V is about 15%, significantly surpassing those of Au/TiO_2 (≈ 8.1%), Au@CeO_x/rGO (≈ 10.1%), and Au nanorods (≈ 4.0%). The NH_3 FE is nearly zero for both commercial 5% Ru/C and $NaBH_4$ reduced Ru on few-layer graphene (FLG). This may be due to the larger sizes of formed Ru (over 3 nm in either case), thus leading to the predominant occurrence of the HER. Whereas when the sizes of Ru are reduced to an atomic level the HER may be suppressed and NH_3 formation promoted. Indeed, the NH_3 yield rates of both Ru@ZrO_2/NC and Ru@NC catalysts are substantially higher than those of Ru@ZrO_2/C and Ru@C in which no amino groups were used during synthesis (Figure 3b), highlighting the importance of the small size of Ru in NRR. The lack of further work using Ru in NRR is likely due to the difficulty in obtaining a high yield of single Ru sites.

We explored the effect of ZrO_2 in the Ru catalysts on NRR. The average NH_3 yield rates and FEs of Ru@NC, Ru@C, Ru@ZrO_2/NC, and Ru@ZrO_2/C at potentials between -0.01 and -0.31 V are plotted in Figure 3c and Figure 3d, respectively. At potentials that are more negative than -0.31 V, the NH_3 FEs fell down to near zero due to serious HER.[21] ZrO_2 itself has very low activity with NH_3 FEs < 4% (Figure S7a), but the addition of ZrO_2 remarkably improved the NH_3 FEs of Ru catalysts at all applied potentials. The NH_3 FEs of Ru@ZrO_2/NC and Ru@ZrO_2/C increased concomitantly with the potential in the range of -0.31 to -0.11 V, and reached a maximum exceeding 13% at -0.11 V in both cases. This contrasts to the maximum NH_3 FEs of less than 9% on Ru/NC and Ru/C in the absence of ZrO_2 at -0.21 V. Notably, the NH_3 FE of Ru@ZrO_2/NC is as high as ~21%, 5 times higher than that of Ru@NC. As far as we are aware, this is the highest NH_3 FE reported so far for aqueous NRR at ambient conditions. Likewise, the NH_3 yield rates and NH_3 partial current densities of Ru@ZrO_2/NC and Ru@ZrO_2/C, with the former outperforming the latter, are higher than those of corresponding catalysts without ZrO_2 at various potentials (Figures 3d and e). The mass activities of the catalysts at the applied potentials followed a similar trend with their NH_3 partial current densities (Figure S7b), further confirming the significant role of ZrO_2 in accelerating NRR to produce NH_3.

The long-term performances of Ru@ZrO_2/NC were evaluated at a constant potential of -0.21 V. The trend of current density curves against time displayed a very stable behavior over 60 h (Figure S7c). Both NH_3 yield rate and FE exhibited almost no changes after 6 consecutive N_2 reduction cycles (Figure S7d) or even 60 h of continuous experimentation (Figure 3f), indicating the excellent stability of Ru@ZrO$_2$/NC for NRR. Experiments were also performed at -0.21 V with N_2 flow rates in a range of 20 to100 cm^3 min^{-1}. No significant effect was observed in both FE and yield rate of NH_3, suggesting that diffusion was unlikely a key step.[11]

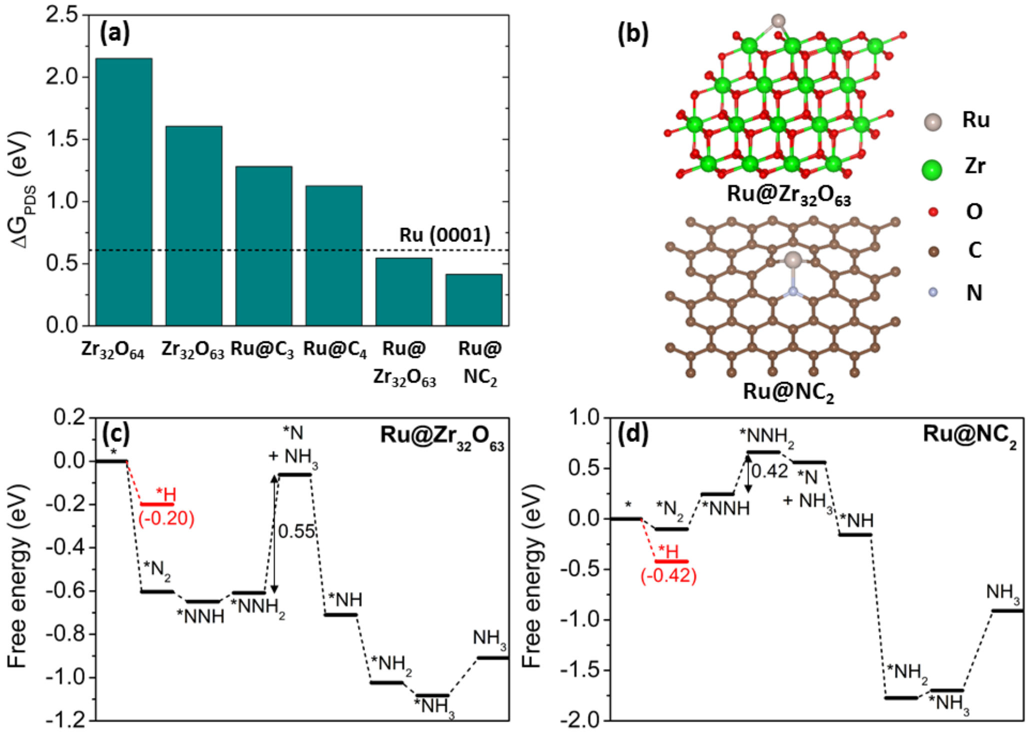

Figure 4. Calculation Models and Free Energy Diagrams for NRR

(a) ΔG_{PDS} for NRR on various reaction sites.

(b) Calculation models for Ru@$Zr_{32}O_{63}$ and Ru/NC_2.

(c) Free energy diagram for NRR on Ru@$Zr_{32}O_{63}$.

(d) Free energy diagram for NRR on Ru@NC_2.

The horizontal dashsed line in (a) represents the ΔG_{PDS} of Ru (0001) (0.61 eV). Stoichiometric ZrO_2 and ZrO_2 with O-vacancy are modelled with $Zr_{32}O_{64}$, and $Zr_{32}O_{63}$, respectively. Asterisk (*) represents a surface site for adsorption. Black and red line indicate free energy change for NRR and hydrogen adsorption, respectively. The free energy change at PDS is denoted in the figure. After the first desorption of NH_3, it is omitted for clarity.

To elucidate the cause of the enhanced catalytic activity and selectivity of Ru@ZrO$_2$/NC, we calculated the reaction free energies for NRR and HER using DFT calculations. Based on the experimental observation of Ru single atom embedded at ZrO_2 and N-doped carbon (Figure 2), we considered single Ru sites supported on both ZrO_2 and N-doped carbon. For Ru single atom at ZrO_2, three cases were modelled; Ru single atom at stoichiometric ZrO_2 (Ru@$Zr_{32}O_{64}$), Zr-vacancy (Ru@$Zr_{31}O_{64}$) and at oxygen-vacancy sites in reduced ZrO_2 (Ru@$Zr_{32}O_{63}$) (Figure 4a and Figure S8).[22,23] We found that the stoichiometric Ru@$Zr_{32}O_{64}$ and Ru@$Zr_{31}O_{64}$ with Zr-vacancy show too high a reaction free energy (> 1 eV) for the first electroreduction step to form *NNH, but Ru@$Zr_{32}O_{63}$ with oxygen-vacancy shows a superior NRR catalytic activity. A previous study on a similar system also indicated that O-vacancy in ZrO_2 surface plays an important role in stabilizing Ru single atom;[22,23] the oxygen vacancy can bind the Ru single atom strongly and reduce the mobility of the anchored Ru single atom significantly, supporting the presence of Ru@$Zr_{32}O_{63}$. Thus, based on the calculated free energy and stability of different single atom configurations considered, we focused here on the results for Ru@$Zr_{32}O_{63}$ with oxygen vacancy.

For Ru single atom at N-doped carbon, we considered Ru@N_xC_y moieties ($0 \leq x \leq 4$ and $0 \leq y \leq 4$) embedded in graphene, where x and y represent the number of anchoring nitrogen and carbon atoms to Ru single atom (Figure S9). Ru@NC_2 was found to show the lowest free energy for NRR among the considered Ru@N_xC_y, and hence we mainly discuss the results for Ru@NC_2. We note that the configuration of Ru@NC_2 is also well matched with the experimental characterizations of Ru/NC in a previous study, which revealed that the Ru atom in Ru/NC has a coordination number of three by extended X-ray absorption fine structure (EAXFS) analyses.[17] The optimized geometries for all reaction intermediates for NRR and HER are shown in Figures S10 and 11. All of these computational results for Ru@ZrO_2 and Ru@NC are then compared with NRR and HER activities of the bulk ZrO_2 and Ru (0001) surfaces, as well as Ru@C_x without N-doping. These comparisons are summarized in Figure 4a and Table S2.

Both Ru single atom catalysts (SACs), Ru@$Zr_{32}O_{63}$ and Ru/NC_2, show improvements in catalytic activity compared to Ru (0001) (Figure 4a), in terms of free energy change at potential determining step (PDS) for NRR; Ru@$Zr_{32}O_{63}$ (0.55 eV) and Ru/NC_2 (0.42 eV) vs. Ru (0001) (0.61 eV). In particular, both Ru SACs, Ru@$Zr_{32}O_{63}$ and Ru/NC_2, reduce the free energy for *NNH formation ($*N_2 + (H^+ + e^-) \rightarrow *NNH$) compared to Ru (0001) by 0.65 and 0.26 eV, respectively (Figures 4c, d and Figure S12), which is usually the most energy consuming step in electrochemical NRR on most metal surfaces, hindering the initiation of NRR process.[4,24] The N_2 adsorption is also favorable on both Ru SACs (ΔG ($*N_2$) being -0.60 and -0.10 eV for @$Zr_{32}O_{63}$ and Ru/NC_2, respectively), to initiate the activation process on both Ru SACs.

On the other hand, support materials themselves (ZrO_2 or ZrO_2 with O-vacancy) do not activate N_2 sufficiently. The free energy change for N_2 adsorption on the bare ZrO_2 surface ($Zr_{32}O_{64}$) is unfavorable (+0.21 eV), and that for *NNH formation is prohibitively high (2.15 eV) (Figure 4a). Similarly, the ZrO_2 with O vacancy ($Zr_{32}O_{63}$), suggested by XPS analyses, itself is also inactive for NRR ($\Delta G_{PDS} = 1.61$ eV). When used as a support material for single Ru atoms, however, $Zr_{32}O_{63}$ enhances the catalytic activity of Ru compared to Ru (0001) as described above, and thus we can conclude that O vacancy sites in ZrO_2 promote the catalytic activity of Ru single atoms in the NH_3 production but does not itself act as a catalyst. We also compared Ru@NC_2 with Ru@C_3 and Ru@C_4 (Figure 4a, Figure S13 and Table S2), which are not involving nitrogen, to investigate the role of N for improved catalytic activity. The ΔG_{PDS} of Ru@NC_2 (0.42 eV) is significantly lower than that of Ru@C_3 (1.28 eV) and Ru@C_4 (1.13 eV). Thus, the unsaturated $-NH_2$ groups not only inhibit aggregation of Ru single atom during pyrolysis[17] but also considerably increases catalytic activity of Ru.

In addition to NRR, we find that the usual H adsorption, which is widely known to adversely block the active sites for NRR and decreases FE in general, is suppressed on both Ru SACs with smaller $\Delta G(*H)$; Ru@$Zr_{32}O_{63}$ (-0.20 eV) and Ru@NC_2 (-0.42 eV) vs. Ru (0001) (-0.47 eV) (Figures 4c and d, and Figure S12). Especially, for Ru@$Zr_{32}O_{63}$, the H adsorption is suppressed most significantly, consistent with the aforementioned selectivity experiments. Comparing $\Delta G(*N_2)$ and $\Delta G(*H)$ might give an approximate idea of the adsorption selectivity. The $\Delta\Delta G(*H/*N_2) = \Delta G(*N_2) - \Delta G(*H)$ for Ru@$Zr_{32}O_{63}$ (-0.40 eV) is much smaller than those for Ru/NC_2 (+0.32 eV) and Ru (0001) (+0.11 eV), suggesting that N_2 adsorption would be less hindered by the H adsorption for Ru@$Zr_{32}O_{63}$ at low overpotential regions.

In Figure 3d, the NH_3 yield rate is similar and most promising for samples that contain both Ru and N-doped carbon sites, namely, for Ru@NC and Ru@ZrO_2/NC. In our DFT calculations, Ru@NC_2 shows the most improved catalytic activity, indicating that Ru@NC_2 sites are likely the origin of the enhanced NH_3 yield rate of Ru@ZrO_2/NC and Ru@NC. On the other hand, Figure 3c shows that FE depends critically on the presence or absence of ZrO_2, suggesting that the NRR/HER selectivity for Ru@ZrO_2/NC is enhanced due to Ru@ZrO_2 or ZrO_2 itself. Our DFT calculations indeed suggest that $*N_2/*H$ selectivity is significantly improved at the Ru@$Zr_{32}O_{63}$ sites, thus plays an important role in the improved FE of Ru@ZrO_2/NC compared to that of Ru@NC. Therefore, in a sense, Ru@ZrO_2/NC seems to show a bifunctional capability in which Ru@NC is mainly responsible for improved NRR while Ru@ZrO_2 helps to suppress HER.

CONCLUSION

In summary, we have demonstrated that single Ru sites supported on ZrO_2/N-doped porous C are highly active in the electroreduction of aqueous N_2 to NH_3. The catalyst afforded a high and stable NH_3 production rate (4560 $\mu g\ h^{-1}\ mg^{-1}_{Ru}$ ·at -0.21 V), as well as very large NH_3 FE (about 21%) with a low overpotential (0.206 V). This outstanding activity correlates with the small size of Ru and the promotion effect of ZrO_2. DFT calculations suggested that the N_2 reduction reaction mainly occurred at Ru sites with oxygen vacancies, and their high catalytic performances can be attributed to the stabilization of *NNH (low overpotential), dramatic destabilization of *H (high NRR/HER selectivity), and enhanced N_2 adsorption (to initiate the NRR process). We believe that the development of single-atom catalysts opens a potentially new avenue for efficient NH_3 synthesis which deserves further research in N_2 fixation.

SUPPLEMENTAL INFORMATION

Supplemental Information includes Supplemental Experimental Procedures, 13 figures, and 2 tables.

ACKNOWLEDGEMENTS

This work was supported by the State Key Laboratory of Organic-Inorganic Composites (No. oic-201503005); the Fundamental Research Funds for the Central Universities (No. buctrc201525); Beijing National Laboratory for Molecular Sciences (BNLMS20160133); Key Laboratory of Materials for High-Power Laser (Shanghai Institute of Optics and Fine Mechanics, CAS). Y.J. acknowledges the support through the National Research Foundation of Korea from the Korean Government (2016M3D1A1021147, 2017R1A2B3010176). AWR acknowledges EPSRC EP/K040375/1, the South of England Analytical Electron Microscope.

AUTHOR CONTRIBUTIONS

H.T. prepared samples and conducted electrocatalytic tests. Z.H., M.J., Q.F., Y.G., and S.L. performed characterizations including XRD, XPS, FTIR, and SEM, etc. C.C. and Y.J. performed DFT calculations. S.H. and A.R made STEM measurements. Z.S. supervised the project and wrote the manuscript. All authors discussed the results and commented on the manuscript.

DECLARATION OF INTERESTS

The authors declare no conflicts of interest.

REFERENCES AND NOTES

1 Honkala, K., Hellman, A., Remediakis, I.N., Logadottir, A., Carlsson, A., Dahl, S., Christensen, C.H., and Norskov, J.K. (2005). Ammonia synthesis from first-principles calculations. Science *307*, 555-558.

2 Li, H., Shang, J., Ai, Z.H., and Zhang, L.Z. (2015). Efficient visible light

nitrogen fixation with BiOBr nanosheets of oxygen vacancies on the exposed {001} facets. J. Am. Chem. Soc. *137*, 6393-6399.

3 Pool, J.A., Lobkovsky, E., and Chirik, P.J. (2004). Hydrogenation and cleavage of dinitrogen to ammonia with a zirconium complex. Nature *427*, 527-530.

4 Montoya, J.H., Tsai, C., Vojvodic, A., and Norskov, J.K. (2015). The Challenge of electrochemical ammonia synthesis: A new perspective on the role of nitrogen scaling relations. ChemSusChem *8*, 2180-2186.

5 Singh, A.R., Rohr, B.A., Schwalbe, J.A., Cargnello, M., Chan, K., Jaramillo, T.F., Chorkendorff, I., and Norskov, J.K. (2017). Electrochemical ammonia synthesis-The selectivity challenge. ACS Catal. *7*, 706-709.

6 Yang, D.S., Chen, T., and Wang, Z.J. (2017). Electrochemical reduction of aqueous nitrogen (N_2) at a low overpotential on (110)-oriented Mo nanofilm. J. Mater. Chem. A *5*, 18967-18971.

7 Li S.J., Bao D., Shi M.M., Wulan B.R., Yan J.M., and Jiang Q. (2017). Amorphizing of Au nanoparticles by CeO_x-RGO hybrid support towards highly efficient electrocatalyst for N_2 reduction under ambient conditions. Adv. Mater. *29*, 1700001.

8 Bao D., Meng F.L., Zhong H.X., Shi M.M., Zhang Y., Yan J.M., Jiang Q., and Zhang X.B. (2017). Electrochemical reduction of N_2 under ambient conditions for artificial N_2 fixation and renewable energy storage using N_2/NH_3 cycle. Adv. Mater. *29*, 1604799.

9 Shi M. M., Bao D., Wulan B. R., Li Y. H., Zhang Y. F., Yan J. M., and Jiang Q. (2017). Au sub-nanoclusters on TiO_2 toward highly efficient and selective electrocatalyst for N_2 conversion to NH_3 at ambient conditions. Adv. Mater. *29*, 1606550.

10 Murakami, T., Nohira, T., Goto, T., Ogata, Y.H., and Ito, Y. (2005). Electrolytic ammonia synthesis from water and nitrogen gas in molten salt under atmospheric pressure. Electrochim. Acta *50*, 5423-5426.

11 Kordali, V., Kyriacou, G., and Lambrou, C. (2000). Electrochemical synthesis of ammonia at atmospheric pressure and low temperature in a solid polymer electrolyte cell. Chem. Commun. 1673-1674.

12 Hiang K.L., Lee Y.H., Liu C., Phang I.Y., Han X.M., Tsung C. K., and Ling X.Y. (2018). Favoring the unfavored: Selective electrochemical nitrogen fixation using a reticular chemistry approach. Sci. Adv. *4*, eaar3208.

13 Lv C.D., Chen G., Yu D., Sun J.X., Zhou Y.S., and Yu G.H. (2018). An amorphous noble-metal-free electrocatalyst enables N_2 fixation under ambient conditions. Angew. Chem. Int. Ed. Doi:10.1002/anie.201801538.

14 Sun, Z.Y., Zhang, X.R., Na, N., Liu, Z.M., Han, B.X., and An, G.M. (2006). Synthesis of ZrO_2-carbon nanotube composites and their application as chemiluminescent sensor material for ethanol. J. Phys. Chem. B *110*, 13410-13414.

15 Chen, S.M., Perathoner, S., Ampelli, C., Mebrahtu, C., Su, D.S., and Centi, G. (2017). Electrocatalytic synthesis of ammonia at room temperature and atmospheric pressure from water and nitrogen on a carbon-nanotube-based

electrocatalyst. Angew. Chem. Int. Ed. *56*, 2699-2703.

16 Back S., and Jung Y.S. (2016). On the mechanism of electrochemical ammonia synthesis on the Ru catalyst. Phys. Chem. Chem. Phys. *18*, 9161-9166.

17 Wang, X., Chen, W.X., Zhang, L., Yao, T., Liu, W., Lin, Y., Ju, H.X., Dong, J.C., Zheng, L.R., Yan, W.S., Zheng, X.S., Li, Z.J., Wang, X.Q., Yang, J., He, D.S., Wang, Y., Deng, Z.X., Wu, Y.E., and Li, Y.D. (2017). Uncoordinated amine groups of metal-organic frameworks to anchor single Ru sites as chemoselective catalysts toward the hydrogenation of quinoline. J. Am. Chem. Soc. *139*, 9419-9422.

18 Zhu C. Z., Shi Q. R., Du D., Lin Y.H. (2017). Single-atom electrocatalysts. Angew. Chem. Int. Ed. *56*, 13944-13960.

19 Zhang, T., Zou, B.H., Shao, M., Chen, X.Y., Zhang, S.Y., Li, L.J., Du, Q.J., Li, H.F., Hu, Y., Weng, J.N., Xiong, W.W., Zheng, B., Zhang, W.N., and Huo, F.W. (2017). Metal-organic framework wears a protective cover for improved stability. Chem. Eur. J. *23*, 7663-7666.

20 Liu Y. M., Quan X., Fan X. F., Chen S., Yu H. T., Zhao H. M., Zhang Y. B., Zhao J. J. (2018). Facile ammonia synthesis from electrocatalytic N_2 reduction under ambient conditions on N-doped porous carbon. ACS Catal. *8*, 1186-1191.

21 Cherevko, S., Geiger, S., Kasian, O., Kulyk, N., Grote, J.P., Savan, A., Shrestha, B.R., Merzlikin, S., Breitbach, B., Ludwig, A., and Mayrhofer, K.J.J. (2016). Oxygen and hydrogen evolution reactions on Ru, RuO_2, Ir, and IrO_2 thin film electrodes in acidic and alkaline electrolytes: A comparative study on activity and stability. Catal. Today *262*, 170-180.

22 Chen, H.Y.T., Tosoni, S., and Pacchioni, G. (2015). Adsorption of ruthenium atoms and clusters on anatase TiO_2 and tetragonal ZrO_2 (101) surfaces: A comparative DFT study. J. Phys. Chem. C *119*, 10856-10868.

23 Chen, H.Y.T., Tosoni, S., and Pacchioni, G. (2015). Hydrogen adsorption, dissociation, and spillover on Ru-10 clusters supported on anatase TiO_2 and tetragonal ZrO_2 (101) surfaces. ACS Catal. *5*, 5486-5495.

24 Skulason, E., Bligaard, T., Gudmundsdottir, S., Studt, F., Rossmeisl, J., Abild-Pedersen, F., Vegge, T., Jonsson, H., and Norskov, J.K. (2012). A theoretical evaluation of possible transition metal electro-catalysts for N_2 reduction. Phys. Chem. Chem. Phys. *14*, 1235-1245.